Diagnosing the influence of diabatic processes on the explosive deepening of extratropical cyclones

Andreas H. Fink, Susan Pohle, Joaquim G. Pinto

Institute for Geophysics and Meteorology, University of Cologne,

Kerpener Str. 13, 50923 Cologne, Germany

Peter Knippertz

School of Earth and Environment, University of Leeds, Leeds, UK

Corresponding Author: Andreas H. Fink, (fink@meteo.uni-koeln.de, Tel.: +49-221 470 3819, FAX: +49-221 470 5161

Note: This is the version of the article as it went to the GRL. Whereas the content will be unchanged, wording changes in the published version may have occurred.

Please cite as follows:

Fink A. H, S. Pohle, P. Knippertz, and J. Pinto, 2012: Diagnosing the influence of diabatic processes on the explosive deepening of extratropical cyclones over the North Atlantic. Geophys. Res. Lett., 39, L07803, doi:10.1029/2012GL051025.

Abstract

A novel version of the classical surface pressure tendency equation (PTE) is applied to ERA-Interim reanalysis data to quantitatively assess the contribution of diabatic processes to the deepening of extratropical cyclones relative to effects of temperature advection and vertical motions. The five cyclone cases selected, Lothar and Martin in December 1999, Kyrill in January 2007, Klaus in January 2009, and Xynthia in February 2010, all showed explosive deepening and brought considerable damage to parts of Europe. For Xynthia, Klaus and Lothar diabatic processes contribute more to the observed surface pressure fall than horizontal temperature advection during their respective explosive deepening phases, while Kyrill and Martin appear to be more baroclinically driven storms. The powerful new diagnostic tool presented here can easily be applied to large numbers of cyclones and will help to better understand the role of diabatic processes in future changes in extratropical storminess.

1. Introduction

Intense cyclones, associated with strong winds and sometimes extreme precipitation, are typical of the mid-latitude winter climate. Recent European wind storms like „Kyrill" in January 2007 [*Fink et al.*, 2009] and „Klaus" in January 2009 [*Liberato et al.,* 2011] led to a large number of fatalities and insured losses of several billion € [*Aon-Benfield*, 2010], as well as to a significant disruption of social activities, public transportation, and energy supply. Large-scale environmental conditions conducive to their development include an unusually strong baroclinic zone associated with an intense jet stream over an extensive longitudinal sector of the North Atlantic [*Pinto et al.*, 2009]. This is particularly true for extreme cyclones, which typically originate off the east coast of North America and propagate towards northern Europe, while secondary developments over the south-eastern North Atlantic are often more "low-level" forced [*Dacre and Gray*, 2009]. The latter suggests a more important contribution from latent heating to rapid cyclogenesis in line with ideas of so called diabatic Rossby waves or vortices [*Parker and Thorpe*, 1995; *Wernli et al.*, 2002; *Moore and Montgomery*, 2005]. In fact, latent heat release and moisture advection from the subtropics apparently played a significant role in the development of storm Klaus in January 2009 [*Knippertz and Wernli*, 2010; *Liberato et al.*, 2011]. *Ulbrich et al.* [2001] and *Pinto et al.* [2009] have shown that strong extratropical cyclones over the Atlantic Ocean are often flanked at their equatorward side with extreme values of the equivalent potential temperature, θ_e, at 850 hPa. This has commonly been interpreted as an indicator of important contributions from latent heat release to cyclone intensification.

The quantification of the relative roles of dry baroclinic vs. moist diabatic processes on the development of the most destructive cyclones is a long standing issue [*Chang et al., 1984*; *Sanders*, 1986; *Wernli et al.*, 2002]. While sensitivity studies using numerical weather prediction (NWP) models can give helpful indications for single cases, a diagnostic framework is needed that can be applied to a wide range of observational and modeling data in various spatial and temporal resolutions. We propose here a novel approach that is based on a careful evaluation of a modified version of the classical pressure tendency equation (PTE) and apply it to five recent strong and destructive European winter storms.

2. Data and Cyclone Tracking

This study is based on ERA Interim Reanalysis data from the European Centre for Medium-Range Weather Forecasts [*Dee et al.*, 2011]. Atmospheric fields were extracted in full temporal (6-hourly) and spatial resolutions (T255; corresponding to a 0.75º grid spacing). Data from the 60 model levels were interpolated onto pressure levels with a vertical spacing of 10 hPa. A standard cyclone detection and tracking scheme based upon the Laplacian of mean sea-level pressure [*Pinto et al.*, 2005] was employed to determine the 6-hourly positions of the surface cyclones.

The diagnostic approach is largely based on the PTE as formulated by *Knippertz and Fink* [2008], and *Knippertz et al.* [2009], which considers a vertical column from the surface to an upper boundary at pressure p_2, here chosen to be 100 hPa (see Auxiliary Material for more details):

$$\underset{Dp}{\frac{\partial p_{sfc}}{\partial t}} = \underset{D\phi}{\rho_{sfc}\frac{\partial \phi_{p_2}}{\partial t}} + \underset{ITT}{\rho_{sfc}R_d\int_{sfc}^{p_2}\frac{\partial T_v}{\partial t}dlnp} + \underset{EP}{g(E-P)} + RES_{PTE} \quad (1)$$

where p_{sfc} is surface pressure, ρ_{sfc} is surface air density, ϕ_{p_2} geopotential at p_2, R_d the gas constant for dry air, T_v the virtual temperature, and g the gravitational acceleration. From left to right the terms denote the surface pressure tendency (Dp), the change in geopotential at the upper boundary (Dϕ), the vertically integrated virtual temperature tendency (ITT), the mass loss (increase) by surface precipitation P (evaporation E; EP), and a residuum due to discretization (RES_{PTE}). With all other terms zero, a lowering of the upper boundary (Dϕ) causes surface pressure fall, as it must be associated with mass evacuation by divergent winds. If the column height remains constant, warming results in horizontal expansion and therefore in a loss of mass (i.e., surface pressure fall). In reality a combination of the two processes is typically found (Figure S1 in Auxiliary Material).

The ITT term in Equation (1) can then be further expanded to (see Auxiliary Material):

$$ITT =$$

$$+\rho_{sfc} R_d \int_{sfc}^{p_2} -\vec{v} \cdot \vec{\nabla}_p T_v dlnp \qquad (TADV)$$

$$+\rho_{sfc} R_d \int_{sfc}^{p_2} \left(\frac{R_d T_v}{c_p p} - \frac{\partial T_v}{\partial p} \right) \omega \, dlnp \qquad (VMT)$$

$$+\rho_{sfc} R_d \int_{sfc}^{p_2} \frac{T_v \dot{Q}}{c_p T} dlnp \qquad (DIAB)$$

$$+RES_{ITT} \qquad (2),$$

where T is temperature, $\vec{v}$ and ω the horizontal and vertical wind components, c_p the specific heat capacity at constant pressure, and $\dot{Q}$ the diabatic heating rate. The first and second terms on the right hand side describe the effects of horizontal temperature advection (TADV) and vertical motions (VMT) on the column-integrated temperature tendency. DIAB contains the influence of diabatic processes such as radiative warming/cooling, latent heat release due to phase changes of water, diffusion, and dissipation. In cloudy areas, like in the core region of extratropical storms, the latent heat release related to microphysical cloud and convective processes is the most important contribution to DIAB, resulting in an atmospheric warming and pressure fall. The term RES_{ITT} represents errors due to discretizations in time and space. The ITT term also includes a small term arising from changes in the humidity content in the column, which is neglected here for reasons explained in the Auxiliary Material.

The application of Equations (1) and (2) using 6-hourly ERA-Interim data is illustrated in Figure 1. The p_{sfc} change between t_{-6h} and t_0 is evaluated over a 3°x3° latitude-longitude box centered on the position of the surface cyclone at t_0. All other terms in Equations (1) and (2) with time tendencies (Dp, Dϕ, and ITT) are also calculated for this box as area- or volume-averaged changes between t_0 and t_{-6h}. The two instantaneous terms (TADV, VMT) are computed by integration over the box volume and then averaging over t_{-6h} and t_0 (Figure 1). This averaging procedure yielded the smallest residua in Equation (2) for an application to the West African heat low using AMMA re-analysis data, for which diabatic tendencies are available [*Pohle,* 2010]. The box is moved along the storm track during the lifetime of the cyclone to create a time series.

Since ERA-Interim does not provide any diabatic tendencies, DIAB had to be calculated as the residuum of Equation (2) and is therefore termed $DIAB_{RES}$. While clearly a limitation of this approach, tests using explicit heating rates show that DIAB and $DIAB_{RES}$ are usually rather similar, though $DIAB_{RES}$ also contains contributions from RES_{ITT} (see Auxiliary Material and *Pohle* [2010]). Further tests varying the upper integration boundary p_2 and the size of the box show that the method is robust (see Auxiliary Material). Finally, the relative contribution of $DIAB_{RES}$ to the total pressure tendency, $DIAB_{ptend}$, is defined by

$$DIAB_{ptend} = \begin{cases} \frac{|DIAB_{RES}|}{|TADV|+|VMT|+|DIAB_{RES}|} * 100, & sgn\,(DIAB_{RES}) = \mathrm{sgn}\,(\mathrm{TADV}) = \mathrm{sgn}\,(\mathrm{VMT}) \\ \frac{|DIAB_{RES}|}{|TADV|+|DIAB_{RES}|} * 100, & sgn\,(DIAB_{RES}) = \mathrm{sgn}\,(\mathrm{TADV}) \wedge sgn\,(DIAB_{RES}) \neq \mathrm{sgn}\,(\mathrm{VMT}) \\ \frac{|DIAB_{RES}|}{|VMT|+|DIAB_{RES}|} * 100, & sgn\,(DIAB_{RES}) = \mathrm{sgn}\,(\mathrm{VMT}) \wedge sgn\,(DIAB_{RES}) \neq \mathrm{sgn}\,(\mathrm{TADV}) \end{cases} \quad (3)$$

3. Selection of storms

The five European winter storms selected to test our methodology are Lothar, Martin (both in December 1999), Kyrill I and II (January 2007, note that Kyrill underwent secondary cyclogenesis over the Atlantic Ocean and thus consists of two cyclone life cycles [*Fink et al.,* 2009]), Klaus (January 2009), and Xynthia (February 2010). All underwent explosive cyclogenesis over the North Atlantic Ocean (see Auxiliary Material) and brought considerable damage to western and central Europe [*Ulbrich et al.*, 2001; *Fink et al.*, 2009; *Liberato et al.,* 2011]. The west-east evolutions of the core mean-sea level pressure as the storms cross the Atlantic Ocean are shown in Figure 2 together with track maps of 300-hPa wind speed and 850-hpa θ_e in a longitudinal moving window centered on the 6-hourly surface position of the storms. All storms (Figures 2a, 2d, 2g, and 2j) except Xynthia (Figure 2m) are associated with a strong polar jet with wind speeds in excess of 160–180 kn, indicating strong baroclinicity. The former storms underwent explosive cyclogenesis during the crossing of the jet polewards (Table S1 and Figures S4–S7 in the Auxiliary Material). Lothar and Klaus are known examples of storms that came under an area of jet-induced upper-level divergence after entering the left exit region while undergoing explosive deepening [*Ulbrich et al.*, 2001; *Liberato et al.,* 2011]. This process is well known to foster rapid development of extratropical cyclones [*Uccellini* 1990]. Xynthia was different in that the storm never crossed the associated polar jet stream (Figure 2m); a split jet configuration might have contributed to the intensification later in its explosive development on 27 February 2010 (Figure S8).

Another factor related to intense cyclogenesis is the ingestion of low-level warm and humid air, transported towards the cyclone's centre ahead of the cold front in the warm conveyer belt [*Browning and Roberts,* 1994]. θ_e at 850 hPa is often used to indicate and track these warm and humid air masses [*Ulbrich et al.*, 2001; *Pinto et al.*, 2009]. Klaus, and especially Xynthia, were associated with extensive areas of θ_e values higher than 320 K at the time when explosive cyclogenesis started (Figures 2k and 2n). Lothar, Martin, and Kyrill I were flanked by lower values and less extensive areas of high θ_e (Figures 2b, 2e, and 2h; see also Figures S4-S8). These analyses allow some qualitative statements as to the potential role of diabatic forcing of the storm deepening. The relative roles of the jet stream (reflecting baroclinic processes) and diabatic heating, however, remain unclear. As will be shown in the next section, such an assessment can be achieved using the PTE.

4. Application of the PTE to five recent Atlantic winter storms

The PTE analysis results are displayed for the five selected winter storms at 6-hourly intervals in Figure 3. The black lines in the left panels show the time evolution of Dp along the storm tracks over the time periods given in the captions of Figure 2. The corresponding segments of the cyclone tracks are colored in the track map shown in Figure S3. It is interesting to compare the evolution of Dp in the left panels of Figure 3 to Figures 2c, 2f, 2i, 2l, and 2o as well as to Table S1. Despite the difference in physical meaning (the latter shows the longitudinal evolution of the core pressures of the cyclone while the former shows the change in pressure in a box fixed in space during the 6 hours the cyclone is approaching) there are some clear structural similarities. This is most obvious for Martin, which deepened only slightly on 25 and 26 December 1999 (Figure 2f) associated with small values of Dp (Figure 3b). On 27 and 28 December the storm went through a period of rapid deepening and subsequent filling, which is well matched by the sharp decrease and subsequent return to small values of Dp. A similarly good correspondence is found for Klaus (Figures 2l and 3d) and Xynthia (Figures 2o and 3e). For Lothar the match between core-pressure changes (Figure 2c) and Dp (Figure 3a) is more complicated due to the dramatic change in propagation speed. During early stages on 24 December 1999, when the storm is rapidly moving across the Atlantic, Dp is on the order of 10 hPa/6 h, although the core pressure is deepening rather slowly. During late stages on 27 December 1999, the cyclone is almost stationary with slowly increasing core pressure and Dp close to zero. For Kyrill the match between core pressure and Dp evolution is somewhat complicated by the two pressure centers, but even here some structural similarities are evident (Figures 2i and 3c).

According to Equation (1) Dp equals the sum of Dϕ, ITT, EP, and RES_{PTE}. For all storms ITT clearly dominates surface pressure changes during most of the lifetime (Figures 3a–e). EP is usually rather small, but reaches almost 2 hPa/6 hrs on 24 December 1999 12–18 UTC (Figure 3a), which is equivalent to 20 mm of box-averaged accumulated rainfall (see Auxiliary Material). At this time, the RES_{PTE} term, which is negligible during most other times, is on the order of 1.3 hPa, pointing to problems with quantitative precipitation forecast in the ECMWF model. A similar behavior is found for the deepening phase of Xynthia (Figure 3e). Dϕ also contributes substantially during some time steps only. The most notable period is the decay of Lothar over Poland and Russia on 26 and 27 December 1999, when Dϕ is relatively large and negative over four time steps (Figure 2a). The sign of Dϕ implies a significant lowering of the 100-hPa surface, which is to some extent compensated by a cooling of the atmospheric column (positive ITT) towards the end of the period. This is in contrast to the four other storms where Dϕ is usually smaller in magnitude and positive. It is likely that this peculiar behavior of Lothar is connected with the movement into the left exit region of the extreme jet over western Europe (Figure 2a), but a detailed study is beyond the scope of this more methodological paper.

The right panels of Figure 3 show the split of the dominant ITT term into TADV, VMT, and $DIAB_{RES}$ (see Equation (2); note the different y axis compared to the left panels). Martin stands out as the system with largest and most constant contributions from VMT ranging between 20 and 40 hPa/6 h (Figure 3g), indicating ascent and adiabatic cooling. Nearly all of this is compensated by similar values of opposite sign associated with TADV. This cancellation, which is found for all other storms as well, is the consequence of air ascending on isentropic surfaces in the area downstream of the cyclone center, where warm advection dominates. Diabatic contributions ($DIAB_{res}$) are relatively small during the early stages of Martin, but increase to more than 20 hPa/6 h during the main deepening phase on 26 and 27 December 1999, during which time they show a similar magnitude to ITT. $DIAB_{RES}$ is again closely related to VMT, as latent heating will depend on ascending motions. However, other factors such as absolute and relative humidity and vertical stability will modify the relation between the two. In order to get an estimate of the relative roles of baroclinic and diabatic contributions, the gray bars at the bottom of each panel show $DIAB_{ptend}$ as defined in Equation 3. We expect $DIAB_{ptend}$ to be more robust than the absolute values of single terms, since they are dependent on factors like storm size, propagation speed, and size of the target box. Over almost all analysis times in Figure 3, $DIAB_{RES}$ is negative, thus $DIAB_{ptend}$ indicates the contribution of diabatic processes to pressure drop. For Martin, $DIAB_{ptend}$ ranges around 30% with highest values towards the end of the deepening phase. From Figure 3, it is evident that VMT is usually of opposite sign to $DIAB_{RES}$ and therefore $DIAB_{ptend}$ is generally calculated using the middle expression of Equation 3. Thus about 70% of the pressure drop during Martin's explosive development is due to horizontal temperature advection, suggesting an overall baroclinically dominated development. Kyrill shows a very similar behavior, although the magnitudes of single terms are somewhat smaller, particularly for Kyrill II (Figure 3g).

The other three storms, Klaus, Xynthia, and Lothar, show substantial contributions from $DIAB_{RES}$ of well above 20 hPa/6 h, leading to $DIAB_{ptend}$ terms of more than 60% due to relatively small contributions from TADV (Figures 3f, 3i, and 3j). The most impressive example is Xynthia.

The large VMT values, which reach similar magnitudes as for Martin during the main deepening phase, are mainly balanced by equally large $DIAB_{RES}$ contributions, while TADV remains largely below 20 hPa/6 h (Figure 3j). This behavior is consistent with the relatively weak jet (Figure 2m) and the high θ_e values in the vicinity of the storm during 26 and 27 February 2010 (Figure 2n). Such simple reasoning, however, does not hold in detail for the other storms. Klaus for example is in the vicinity of a very intense jet on 22 January 2009 (Figure 2j), but TADV contributions are small (Figure 3i). On the other hand $DIAB_{RES}$ contributions are largest on 23 January 2009, when Klaus has already left the area of highest θ_e (Figure 2k). In addition, Lothar has the strongest jet (Figure 2a) of all cases studied here, yet TADV is relatively small throughout most of the development (Figure 3f). θ_e on the other hand is high during the early stages associated with particularly large values of $DIAB_{ptend}$, which is consistent with ideas of diabatic Rossby waves as discussed in *Wernli et al.* [2002]. These results suggests that the details of the state of development of the cyclone, the interactions with the baroclinic zone, and the actual realization of latent heating from high-θ_e air are crucially important for determining VMT, TADV, and $DIAB_{res}$. The sole existence of a strong jet or high-θ_e air is not sufficient to deduce the relative roles of baroclinic vs. diabatic processes.

5. Summary and conclusions

The relative roles of baroclinic and diabatic processes for explosive deepening of extratropical cyclones have been debated for a long time, mostly on the basis of case studies. Here we presented a powerful diagnostic approach to the problem, which is based on a combination of an automatic cyclone tracking with a special version of the classical PTE that relates changes in surface pressure to contributions from horizontal temperature advection and vertical motion as well as to diabatic processes, i.e., mainly latent heat release in clouds. Along the entire track, the PTE is evaluated in a 3°x3° box from the surface to 100 hPa centered on the location the storm is moving to within the next time step. The great advantage of this new approach is the easy applicability to large gridded datasets, even if diabatic tendencies are not explicitly available as in many reanalysis products.

The strengths and limitations of the method are illustrated here through application to five explosively deepening winter storms over the North Atlantic Ocean (Lothar, Martin, Kyrill, Klaus, and Xynthia), which all caused considerable damage in Europe. Data used are 6-hourly ERA-Interim re-analyses. For enhanced interpretation of the results, the PTE analysis was complemented with other classical cyclogenetic factors, i.e., the strength of the polar jet and θ_e at 850 hPa in the warm sector [*Pinto et al.*, 2009]. The main conclusions from this analysis are:

- The time evolutions of the actual core pressure of the storm and the 6-hourly pressure changes in the moving box used to evaluate the PTE show structural similarities that are dominated by the explosive deepening.
- The pressure changes largely follow the net virtual temperature change in the box with only short periods, when vertical movements of the upper lid of the box contribute substantially, as for example during the decay of Lothar.
- The vertical motion term (VMT) is positive throughout the entire lifecycle of all storms indicating the dominance of ascent downstream of the cyclone center.
- VMT is (over-)compensated by negative contributions through warm temperature advection (TADV) and diabatic heating ($DIAB_{res}$), whose relative importance vary strongly during the lifetime of the storms and from system to system.
- Martin and Kyrill appear to be dominated by baroclinic processes with contributions of TADV to the total negative pressure tendencies of around 70%.
- Despite comparable jet strengths, a similar track relative to the jet, and equally high θ_e values at 850 hPa in the warm sector, Lothar and Klaus show much larger diabatic contributions to the negative pressure tendency of around 60% over a 2.5 day period.
- Xynthia stands out as a system with an unusual SW–NE track into Europe, which appears to have benefited from a complicated split jet structure in the later development stages. It is also associated with high θ_e values and shows very large diabatic contributions.
- The PTE results indicate that θ_e in the warm sector and the jet strength alone are not sufficient to

make an assessment of the relative importance of baroclinic and diabatic processes, but that a more elaborate analysis is needed to make this judgment.

Future work should deepen this analysis further by looking more closely into individual times and PTE terms. Particularly for Xynthia, Klaus, and Lothar a comparison with sensitivity experiments, in which diabatic processes are suppressed in a numerical model, would be interesting to confirm the PTE results. In addition it should also be tested to what extent the diabatic term is sensitive to the model and data assimilation system by comparing with other analysis products. More studies on the sensitivity of results to storm diameter, translation speed, box size, and analysis time steps are also needed. In the long run, the PTE analysis will be applied to longer timeseries from both reanalysis and climate model data to generate robust statistics across a broader range of cyclone intensities and development types. This will for the first time allow a systematic investigation of the relative contribution of diabatic processes to storm intensification in recent and future climate conditions, going much beyond the case studies found in the literature so far.

Acknowledgments

We thank the European Centre for Medium-Range Weather Forecasts for the use of the ERA Interim Reanalysis dataset. JGP thanks AON Benfield Impact Forecasting for support over the EUWS project. PK acknowledges funding from the AXA Research Fund for the SEAMSEW project. We wish to thank Thomas Engel, Tomek Trzeciak and Jenny Owen for help in creating Figure 3. Finally we are grateful to Steve Dorling and one anonymous Reviewer for their comments that greatly helped to improve the manuscript.

References

Aon-Benfield (2010), Annual global climate and catastrophe report IF 2009, online available at http://www.aon.com.

Browning, K. and N. M. Roberts (1994), Structure of a frontal cyclone, *Quart. J. Roy. Meteor. Soc.,* *120,* 1535–1557.

Chang C. B., D. J. Pepkey, and C. W. Kreitzberg (1984), Latent heat induced energy transformations during cyclogenesis, *Mon. Weather Rev., 112,* 357–367.

Dacre, H. F., and S. L. Gray (2009), The spatial distribution and evolution characteristics of North Atlantic cyclones, *Mon. Weather Rev., 137,* 99–115.

Dee, D., and co-authors (2011), The ERA-Interim reanalysis: configuration and performance of the data assimilation system, *Quart. J. Roy. Meteor. Soc., 137,* 553–597.

Fink, A. H., T. Brücher, E. Ermert, A. Krüger, and J. G. Pinto (2009), The European storm Kyrill in January 2007: Synoptic evolution, meteorological impacts and some considerations with respect to climate change, *Nat. Hazards Earth Syst. Sci., 9,* 405–423, doi:10.5194/nhess-9-405-2009.

Knippertz, P. und A. H. Fink (2008), Dry-season precipitation in tropical West Africa and its relation to forcing from the extratropics, *Mon. Weather Rev., 136,* 3579–3596.

Knippertz, P., A. H. Fink, and S. Pohle (2009), Reply, *Mon. Weather Rev.,* 137, 3151–3157.

Knippertz, P., and H. Wernli (2010), A Lagrangian climatology of tropical moisture exports to the Northern Hemispheric extratropics, *J. Climate, 23,* 987–1003.

Liberato M. R. L., J. G. Pinto , I. F. Trigo, and R. M. Trigo (2011), Klaus - an exceptional winter storm over Northern Iberia and Southern France, *Weather, 66,* 330–334, doi:10.1002/wea.755.

Moore, R. W., and M. T. Montgomery (2005), Analysis of an idealized, three-dimensional diabatic Rossby vortex: a coherent structure of the moist baroclinic atmosphere, *J. Atmos. Sci., 62,* 2703–2725.

Parker, D. J., and A. J. Thorpe (1995), Conditional convective heating in a baroclinic atmosphere: A model of convective frontogenesis, *J. Atmos. Sci., 52,* 1699–1711.

Pinto, J. G., T. Spangehl, U. Ulbrich, and P. Speth (2005), Sensitivities of a cyclone detection and tracking algorithm: individual tracks and climatology, *Meteorol. Z., 14*, 823–838, doi:10.1127/0941-2948/2005/0068.

Pinto J. G., S. Zacharias, A. H. Fink, G. C. Leckebusch, and U. Ulbrich (2009), Factors contributing to the development of extreme North Atlantic cyclones and their relationship with the NAO, *Clim. Dyn., 32,* 711–737, doi: 10.1007/s00382-008-0396-4.

Pohle, S. (2010), Synoptische und dynamische Aspekte tropisch-extratropischer Wechselwirkungen: Drei Fallstudien von Hitzetiefentwicklungen über Westafrika während des AMMA-Experiments 2006 (In German). Ph.D. thesis at the University of Cologne, Germany, online available at http://kups.ub.uni-koeln.de/volltexte/2010/3157/pdf/DissertationSusanPohle2010.pdf.

Sanders F. (1986), Explosive cyclogenesis in the West-Central North Atlantic Ocean, 1981–84. Part I: Composite structure and mean behavior, *Mon. Weather Rev., 114,* 1781–1794.

Uccellini, L. W. (1990), Process contributing to the rapid development of extratropical cyclones, In: Extratropical Cyclones: The Eric Palmen Memorial Volume, edited by: Newton, C. and Holopainen, E., Am. Meteorol. Soc., 81–107.

Ulbrich, U., A. H. Fink, M. Klawa, and J. G. Pinto (2001), Three extreme storms over Europe in December 1999, *Weather, 56,* 70–80.

Wernli H., S. Dirren, M. A. Liniger, and M. Zillig (2002), Dynamical aspects of the life-cycle of the winter storm `Lothar' (24-26 December 1999), *Quart. J. Roy. Meteor. Soc., 128,* 405–429.

Figure Captions:

Figure 1: Relative Schematic illustration of the methodology (see Section 2 for details and definition of terms). The bold arrow in the x-y plane indicates the motion of the center of a surface cyclone between two analysis times t_0 and t_{-6h} (arrow length not true to the scale). The surface pressure tendency equation is evaluated for the 3°x3° latitude-longitude box extending from the surface to 100 hPa centered on the position of the storm at t_0. The terms of Equation (2), TADV (horizontal advection; red arrows) and VMT (vertical advection; dark blue vectors), are computed by integrating over the box volume and then averaging over t_0 and t_{-6h} as schematically indicated in the two graphs in the top right corner. The computation of the terms Dϕ, Dp, DIAB (diabatic processes; curled orange vectors), and EP (evaporation minus precipitation; curled blue vectors and

dashed blue lines) is illustrated in the lower four graphs on the right-hand side. Note that while Dϕ and Dp are simple differences between instantaneous values at t_0 and t_{-6h}, EP is the difference between two parameters accumulated between t_0 and t_{-6h}. $DIAB_{RES}$ is the residuum of Equation (2).

Figure 2: Characteristics of investigated storms. (a) 6-hourly track of storm Lothar between 0000 UTC 24 and 1200 UTC 28 December 1999 together with wind speed [Kn] at 300 hPa in a longitudinal window centered on the surface position of the storm. (b) As (a) but for θe [K] at 850 hPa. (c) 6-hourly core pressure development of Lothar plotted against longitude. The red part of the pressure curve denotes the period of explosive deepening as in Table S1. The other panels show corresponding analyses for (d)–(f) Martin 0600 UTC 24 – 1800 UTC 29 December 1999, (g)–(i) Kyrill I and II 0600 UTC 15 – 1800 UTC 20 January 2007, (j)–(l) Klaus 1200 UTC 21 – 1800 UTC 26 January 2009, and (m)–(o) Xynthia 1800 UTC 25 February – 1200 UTC 03 March 2010. The calendar days along the tracks correspond to 0000-UTC positions. Note the slightly different geographical areas of the horizontal distributions.

Figure 3: Results of the PTE analysis. Left/Right panels: Terms of Equation (1)/(2) for the storms (a)/(f) Lothar, (b)/(g) Martin, (c)/(h) Kyrill I and II, (d)(i) Klaus, and (e)/(j) Xynthia. For an explanation of the different terms, see section 2. In the right panels, DIABptend (gray bars in %, scale on right y-axis) is defined as in Equation 3. Note the different pressure scales in the left and right panels. The vertical bold lines delineate the interval of explosive deepening as in Table S1. The periods correspond to those in the captions of Figure 2 (see also Figure S3).

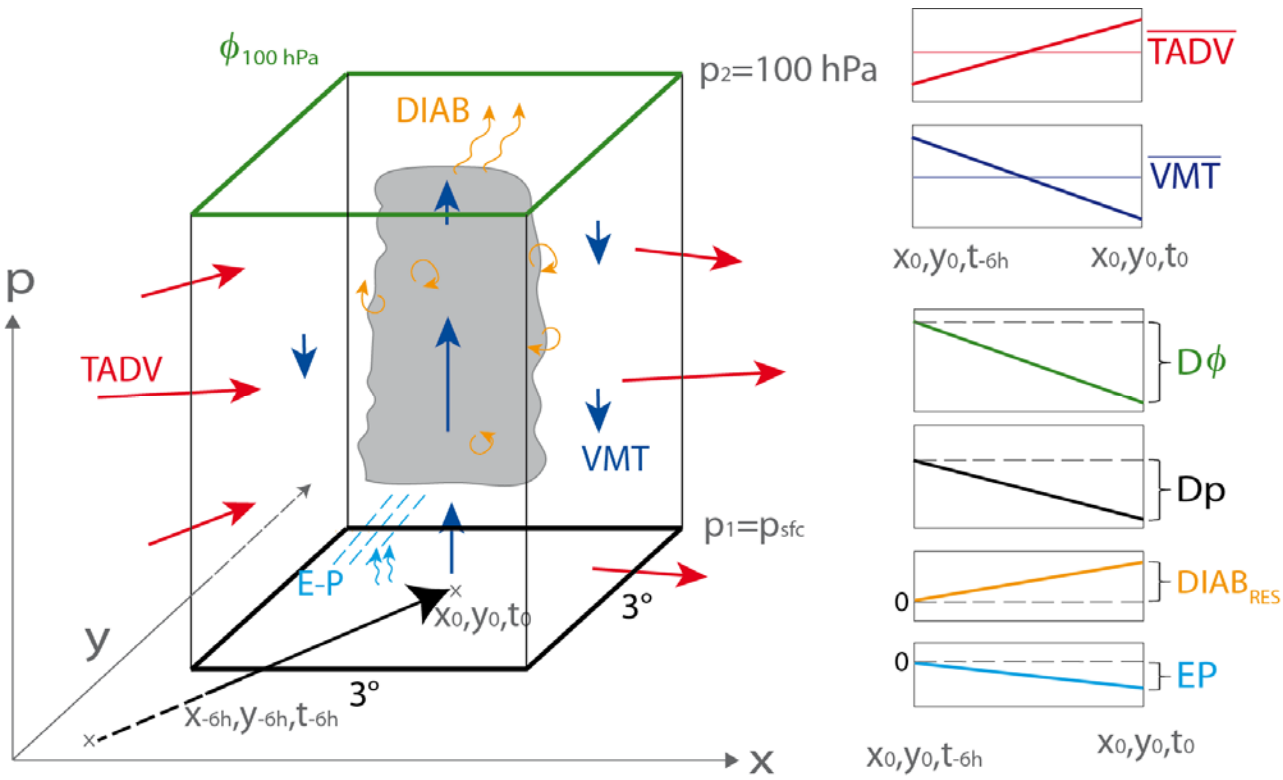

Figure 1. Schematic illustration of the methodology (see Section 2 for details and definition of terms). The bold arrow in the x-y plane indicates the motion of the center of a surface cyclone between two analysis times t_0 and t_{-6h} (arrow length not true to the scale). The surface pressure tendency equation is evaluated for the 3°x3° latitude-longitude box extending from the surface to 100 hPa centered on the position of the storm at t_0. The terms of Equation (2), TADV (horizontal advection; red arrows) and VMT (vertical advection; dark blue vectors), are computed by integrating over the box volume and then averaging over t_0 and t_{-6h} as schematically indicated in the two graphs in the top right corner. The computation of the terms $D\phi$, Dp, DIAB (diabatic processes; curled orange vectors), and EP (evaporation minus precipitation; curled blue vectors and dashed blue lines) is illustrated in the lower four graphs on the right-hand side. Note that while $D\phi$ and Dp are simple differences between instantaneous values at t_0 and t_{-6h}, EP is the difference between two parameters accumulated between t_0 and t_{-6h}. $DIAB_{RES}$ is the residuum of Equation (2).

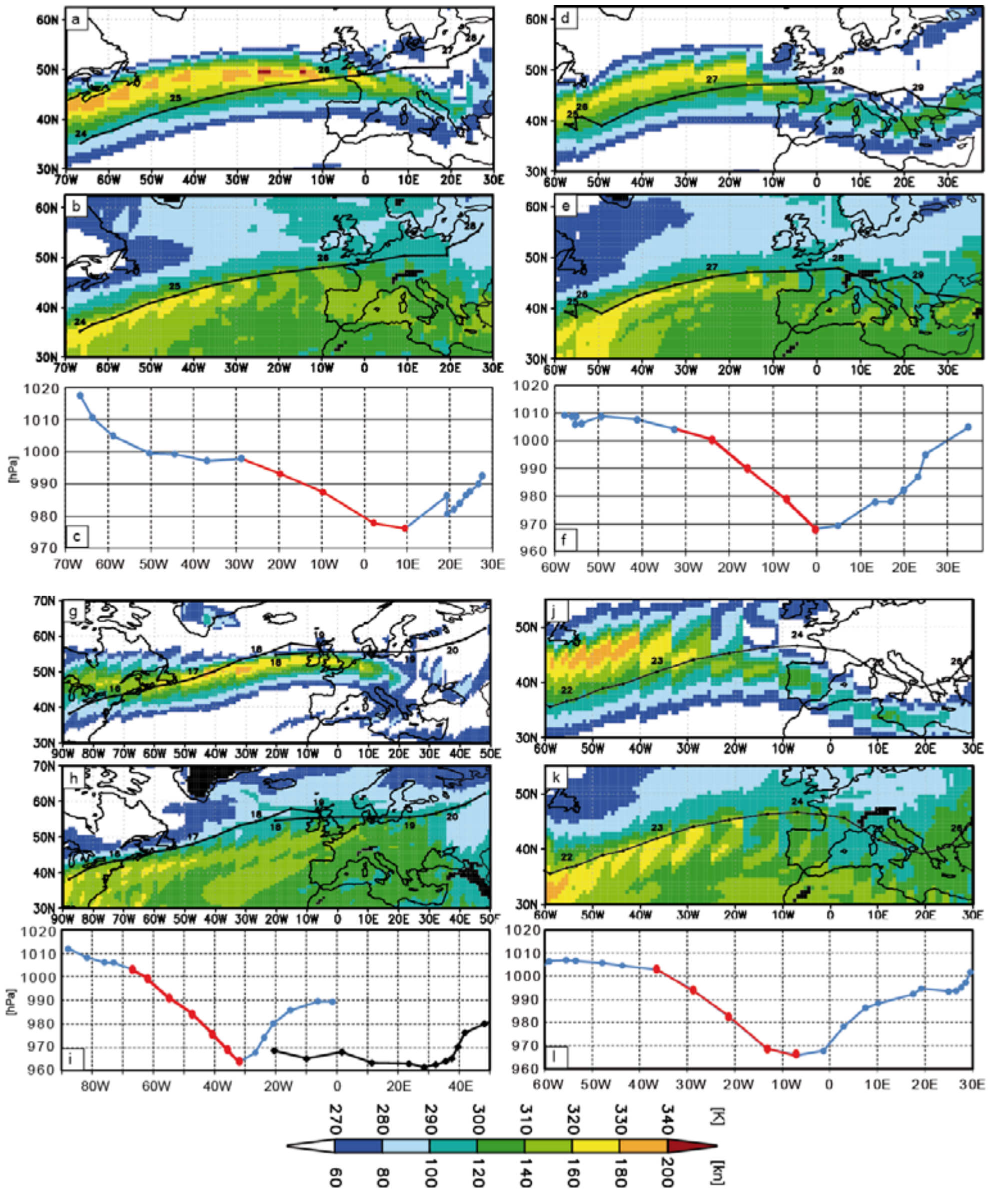

Figure 2. Characteristics of investigated storms. (a) 6-hourly track of storm Lothar between 0000 UTC 24 and 1200 UTC 28 December 1999 together with wind speed [Kn] at 300 hPa in a longitudinal window centered on the surface position of the storm. (b) As (a) but for θ_e [K] at 850 hPa. (c) 6-hourly core pressure development of Lothar plotted against longitude. The red part of the pressure curve denotes the period of explosive deepening as in Table S1. The other panels show corresponding analyses for (d)–(f) Martin 0600 UTC 24 – 1800 UTC 29 December 1999, (g)–(i) Kyrill I and II 0600 UTC 15 – 1800 UTC 20 January 2007, (j)–(l) Klaus 1200 UTC 21 – 1800 UTC 26 January 2009, and (m)–(o) Xynthia 1800 UTC 25 February – 1200 UTC 03 March 2010. The calendar days along the tracks correspond to 0000-UTC positions. Note the slightly different geographical areas of the horizontal distributions.

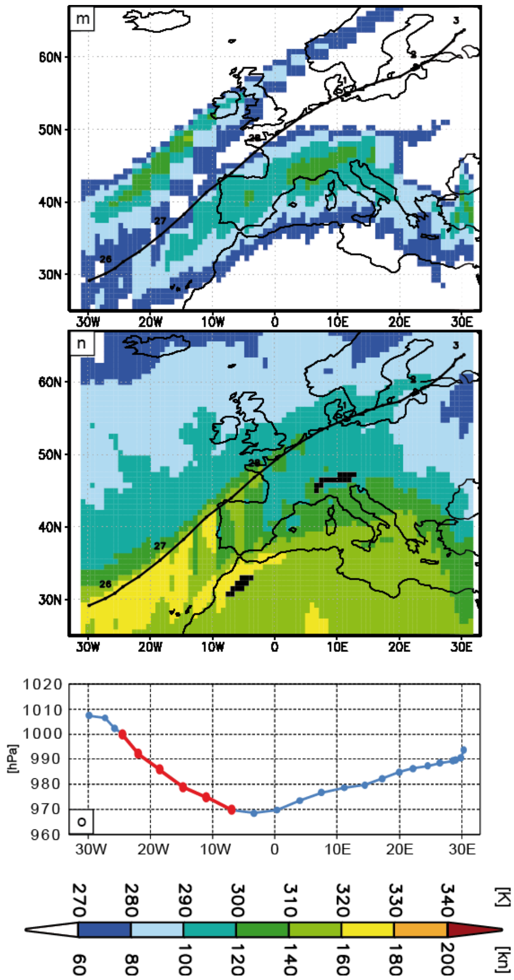

Figure 2. (continued).

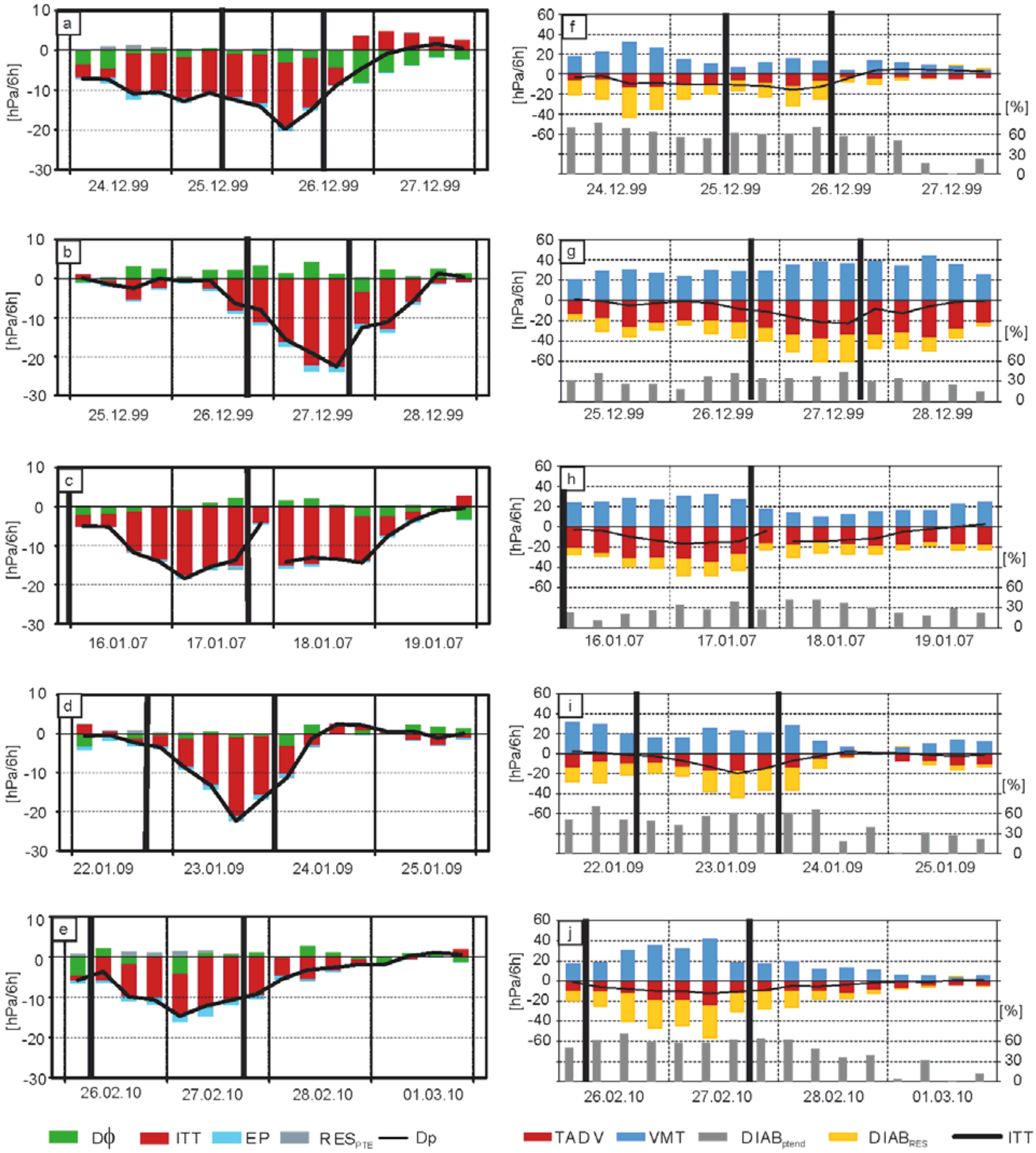

Figure 3. Results of the PTE analysis. Left/Right panels: Terms of Equation (1)/(2) for the storms (a)/(f) Lothar, (b)/(g) Martin, (c)/(h) Kyrill I and II, (d)/(i) Klaus, and (e)/(j) Xynthia. For an explanation of the different terms, see section 2. In the right panels, $DIAB_{ptend}$ (gray bars in %, scale on right y-axis) is defined as in Equation 3. Note the different pressure scales in the left and right panels. The vertical bold lines delineate the interval of explosive deepening as in Table S1. The periods correspond to those in the captions of Figure 2 (see also Figure S3).

Diagnosing the influence of diabatic processes on the explosive deepening of extratropical cyclones

by A. H. Fink, S. Pohle, J. G. Pinto, and P. Knippertz

- Auxiliary Material –

1. Derivation, Application and Interpretation of the Pressure Tendency Equation

Knippertz and Fink [2008] used the pressure tendency equation (PTE) in a form similar to the one discussed in the main paper to investigate the role of the wintertime surface heat-low dynamics for dry-season precipitation over West Africa. However, the impact of rain/surface evaporation and changes in humidity, including state phases of water by melting/freezing, condensation/evaporation, sublimation/re-sublimation, and their horizontal/vertical transports in the air column were not taken into account. Additionally, in accordance with many earlier studies, the existence of a so-called level of insignificant dynamics (LID), where the geopotential height is nearly constant at the upper integration boundary [*Hirschberg and Fritsch*, 1993], was assumed. However, the LID concept was later questioned by *Spengler and Egger* [2009] and shown not to be applicable, at least for the West African heat low case [*Knippertz et. al.*, 2009]. As a consequence, an extended PTE is used here, in which changes of the geopotential at the top of the column, the effect of net evaporation minus precipitation on the mass in the column, and mass changes due to vertical changes in water vapor are considered. The latter was found to be the dominant term in the humidity contributions. The first step of the derivation is based upon the hydrostatic and the continuity equations (a step-by-step derivation is presented in *Pohle* [2010, Chapters 4.1-4.3]).

$$\frac{\partial}{\partial z}\left(\frac{1}{\rho}\frac{\partial p}{\partial t}\right) = -\frac{g}{\rho}\left(\frac{\partial \rho}{\partial t}\right) = \frac{g}{\rho}\left(\vec{v}\vec{\nabla}_p\rho + \omega\frac{\partial \rho}{\partial p} - \frac{d\rho}{dt}\right) \qquad (S1),$$

with the density ρ, the acceleration of gravity g, pressure p, and the horizontal and vertical wind components $\vec{v}$ and ω. Using $p = \rho R_d T_v$, with the gas constant R_d, and the first law of thermodynamics, the terms on the right-hand side can be written as functions of the virtual temperature, T_v:

$$g\ \frac{1}{\rho}\vec{v}\vec{\nabla}_p\rho = -g\frac{\vec{v}}{T_v}\vec{\nabla}_p T_v \qquad (S2)$$

$$g\ \frac{1}{\rho}\omega\frac{\partial\rho}{\partial p} = -g\frac{\omega}{p}\left(1+\frac{R_d}{g}\cdot\frac{\partial T_v}{\partial z}\right) \qquad (S3)$$

$$g\ \frac{1}{\rho}\frac{d\rho}{dt} = g\left(\left(1-\frac{R_d}{c_p}\right)\cdot\frac{\omega}{p}-\frac{\dot{Q}}{c_pT}-\frac{T}{T_v}\cdot 0.608\cdot\frac{dq}{dt}\right) \qquad (S4),$$

where T is the dry temperature, c_p the specific heat capacity at constant pressure, and $\dot{Q}$ representing the diabatic heating rate. The next steps are: the insertion of the three terms S2, S3, and S4, the exchange of $g \cdot dz$ by $\frac{1}{\rho}\cdot dp$ and integration form surface *sfc* to the upper boundary p_2, the replacement of the pressure tendency at the upper boundary (height coordinates) by the geopotential tendency (pressure coordinates), and the consideration of the influences of precipitation and evaporation to the surface pressure. Thus the pressure tendency equation becomes:

$$\frac{\partial p_{sfc}}{\partial t} = \qquad (D\mathrm{p})$$

$$\rho_{sfc}\frac{\partial \phi_{p_2}}{\partial t} \qquad (D\Phi)$$

$$+\rho_{sfc}R_d\int_{sfc}^{p_2} -\vec{v}\cdot\vec{\nabla}_p T_v dlnp \qquad (TADV)$$

$$+\rho_{sfc}R_d\int_{sfc}^{p_2}\left(\frac{R_dT_v}{c_pp}-\frac{\partial T_v}{\partial p}\right)\omega\, dlnp \qquad (VMT)$$

$$+\rho_{sfc}R_d\int_{sfc}^{p_2} 0.608\cdot T\frac{dq}{dt}dlnp \qquad (HUM)$$

$$+\rho_{sfc}R_d\int_{sfc}^{p_2}\frac{T_v\dot{Q}}{c_pT}dlnp \qquad (DIAB)$$

$$+g(E-P) \qquad (EP) \qquad (S5)$$

The net temperature advection (TADV), the vertical motion multiplied by the static stability (VMT), the net total change of the water vapor content q (HUM), and diabatic processes (DIAB) represent the processes causing virtual temperature changes in an air column. The last term, EP, describes the influence of rain and evaporation on Dp; in the occurrence of precipitation, the pressure falls due to the mass loss reduced by the surface evaporation. For example, a mean 6-hourly accumulated precipitation of 10 mm within our 3°x3° box is equivalent to the removal of 10 kg m^{-2} of mass. Neglecting evaporation, this corresponds to a change in weight per unit area of about 100 N and thus a change in surface pressure of 100 Pa or 1 hPa. Note that changes of specific humidity q cause density changes that can be expressed in terms of temperature changes. Thus the PTE can be written in a short form as (cf. *Pohle* [2010], her Equation 4.23):

$$\underbrace{\frac{\partial p_{sfc}}{\partial t}}_{Dp} = \underbrace{\rho_{sfc}\frac{\partial \phi_{p_2}}{\partial t}}_{D\phi} + \underbrace{\rho_{sfc}R_d\int_{sfc}^{p_2}\frac{\partial T_v}{\partial t}dlnp}_{ITT} + \underbrace{g(E-P)}_{EP} \qquad (S6),$$

where Dp denotes the surface pressure tendency and Dϕ the changes of the geopotential at the upper boundary of the column. ITT represents the net temperature tendency in a column, integrated from the bottom to the defined top level.

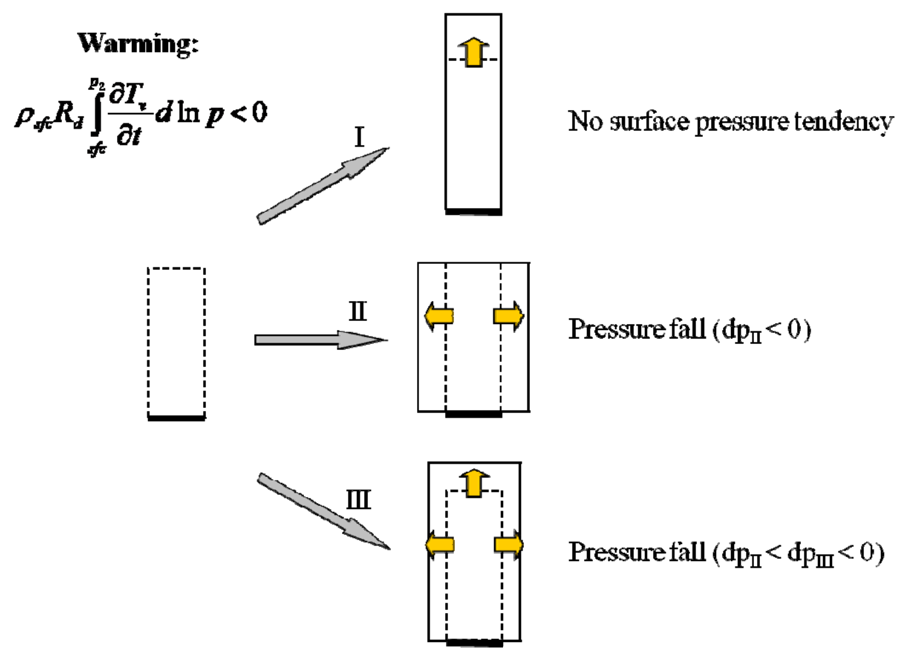

Figure S1. Illustration of the possible deformations of an air column due to warming. Firstly, the heating is completely transferred into the lifting of the upper boundary (hypsometric equation). Thus no mass evacuation occurs and therefore no surface pressure tendency. Secondly, the column height remains constant, whereas the heating is completely transferred into surface pressure fall (by mass evacuation due to divergent winds). Thirdly, the effect of column heating is separated into the lifting of the upper boundary and mass evacuation.

To understand which processes cause a pressure change, no rain or surface evaporation is assumed (EP=0). The warming or cooling of air within the column related to the ITT term in Equation S6 expands or compresses it. In case of pure vertical expansion/compression (sketch I in Figure S1), the upper boundary of the column lifts/falls, which means a rising/descending of the geopotential of the same order. No mass change in the column and therefore no pressure change occur. In contrast, a pure horizontal extension/compression (sketch II in Figure S1) due to warming/cooling (ITT in Equation S6 positive/negative) causes a mass reduction/increase in the air column over a defined area, in conjunction with a constant top level, which means no geopotential changes ($D\phi=0$). In reality a mixture of the two cases is observed (sketch III in Figure S1).Without any temperature changes (ITT=0), surface pressure changes are possible in cases of pure dynamical mass convergence and related changes in the geopotential at the top of the column ($D\phi$ in Equation S6).

The various processes resulting in a warming or cooling of the column (i.e., nonzero ITT) are as follows. The kinematic terms, TADV and VMT, have opposing contributions to the surface pressure fall, i.e., warm air advection (TADV<0, contribution to pressure fall) causes lifting (VMT>0, contribution to pressure rise) and vice versa. Changes in humidity content (HUM, see Equations 4.29 and 4.31 in *Pohle* [2010] for a full formulation of the HUM term including all state phases of water) are dominated by horizontal and vertical transports of water vapor. Thus, we neglected the total changes of ice and liquid water. In this context, the HUM term can be understood as the effect of water vapor on the density of air at different temperatures: If a given amount of water vapor is transported upward from a level with higher temperatures to a higher level with lower temperatures, the virtual temperature sinks more at the lower level due to the water vapor loss than it rises at the upper level due to the water vapor gain. A net cooling occurs in connection with low-level convergence and less mass divergence above. Thus, the density increase as a net effect and therefore the pressure rises. Note, however, that the HUM term, neglecting solid phases of water and horizontal transports, was negligible for all five storms. Therefore, it is not considered in the main text.

The term DIAB contains the consequence of diabatic processes, such as radiative warming/cooling, latent heat release due to condensation, diffusion, and dissipation. In the case of no clouds and at night, radiative processes dominate the other diabatic processes; especially at night the atmosphere cools due to outgoing longwave radiation contributing to pressure rise. In cloudy areas the latent heat release related to microphysical cloud and convective processes is important and results in an atmospheric warming and pressure fall.

In the case of no available diabatic heating profiles from an analysis or model archive, *Pohle* [2010] demonstrated for West African heat low cases in 2006, for which strong radiative and convective contributions to DIAB existed, that meaningful results are obtained if the DIAB term is calculated as the residuum of Equation S5 (termed $DIAB_{res}$ in the main text). This comparison was made possible by the fact that the AMMA reanalysis had a special archive with 6-hourly explicit diabatic tendencies such that DIAB could be calculated and compared to $DIAB_{res}$ from ERA-Interim; the result showed a surprisingly good agreement.

Critical to the PTE-based analyses of surface pressure changes is the choice of the upper integration boundary p_2. The sensitivity of the values of the vertical integrals against p_2 was tested. It was found that in almost all cases and analysis times, the integrals remained nearly constant for upper integration boundaries above the local tropopause. This is shown for Klaus and Martin in Figure S2. Therefore, p_2 was set to 100 hPa, above typical heights for extratropical tropopauses. Such a test should always be made before applying the pressure tendency equation since in the West African heat low area such a quasi-constant integral value for upper integration boundaries above the tropopause level was not found.

Due to the spatiotemporal discretization, neither Equation S5 nor S6 are closed. Firstly, Dp and $D\phi$ are tendencies at one level, on the other hand ITT denotes an integral. Secondly, time-dependent and instantaneous terms are included. To close Equations S5 and S6, the terms RES_{ITT} and RES_{PTE} have been added to Equations (1) and (2) in the main text. Thus, $DIAB_{res}$ also contains contributions from RES_{ITT}, but again we note the good agreement found for the diabatic terms when calculated with explicit diabatic terms and as a residual for the West African heat low region.

Finally, tests with a 1.5°x1.5° box yielded qualitatively similar results though the terms had higher values for the smaller box. The lack of higher time resolution in the analyses made it impossible to test the sensitivity results against the analyses time step.

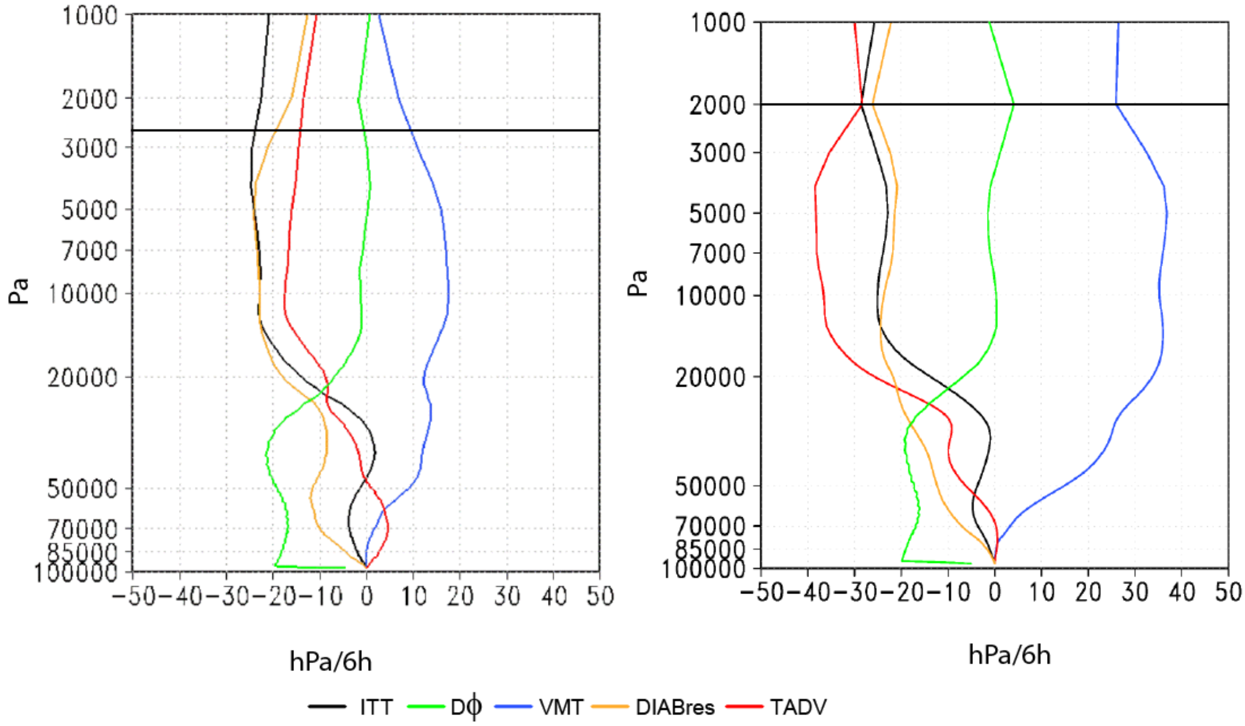

Figure S2. Pressure-level profiles of the right hand side terms in Equations (1) and (2) of the main text depending on the upper integration boundary. Shown are results for Klaus 23 Jan. 2009 12-18 UTC (left panel) and Martin for the period 27 Dec. 1999 12-18 UTC (right panel). The black horizontal line indicates the local tropopause. Note that DIABres corresponds to DIAB+Res_{ITT} in Equation (2).

2. Properties of the five selected winter storms

Figure S3 shows the six-hourly surface tracks of cyclones Lothar, Martin (both in December 1999), Kyrill (January 2007), Klaus (January 2009), and Xynthia (February 2010). Klaus, Lothar, and Martin have almost overlapping tracks before landfall in western France. Kyrill took a more northerly route and re-developed over the eastern North Atlantic from a secondary cyclogenesis [*Fink et al.*, 2009]. As a consequence, the tracks of Kyrill I and II are displayed in Figure S3. The track of the most recent storm Xynthia in February 2010 is worthy of note for two reasons: (a) its unusual origin in the eastern subtropical Atlantic Ocean and (b) its atypical southwest-northwest orientation compared to the climatology [cf. *Pinto et al*., 2009].

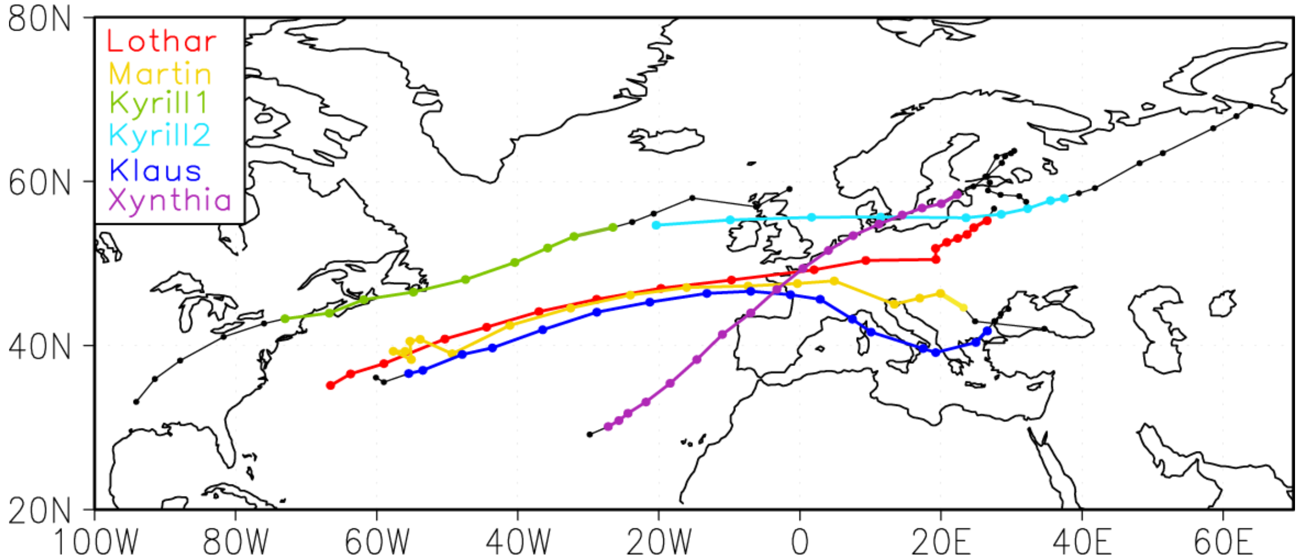

Figure S3. Six-hourly surface tracks of investigated storms based on the location of the core pressure in mean sea-level pressure from ERA Interim analyses. Cyclones Lothar (in red), Martin (in orange), Kyrill I and II (green and light blue), Klaus (dark blue), and Xynthia (purple). The colored parts of the tracks correspond to the dates shown in Figures 2 of the main text; the remaining segments of the tracks are displayed in black.

For the period of explosive cyclone intensification, Table S1 shows the six-hourly latitude-longitude positions, minimum mean sea-level pressures (MSLP) as derived from ERA Interim, and corresponding MSLP tendencies (dMSLP) for the last 6 hours of the five storms discussed in the main text. The last column gives the latitude dependent 24-h threshold for explosive cyclone deepening according to *Lim and Simmonds* [2002]. In this way, it is possible to directly identify if explosive development occurred by adding the dMSLP changes over 24 hours (e.g., -21.74 hPa for Lothar 18 UTC 25 Dec 1999 through 12 UTC 26 Dec. 1999). Analysis times before minimum core mean-sea level pressure have been selected for which the 24h criterion of explosive cyclone deepening is fulfilled. Note that minimum MSLP in analyzed surface weather charts or observed at weather stations might be lower than in ERA Interim due to the moderate (~ 75 km) resolution or due to rejection of extreme tendencies/values from station observations by the ERA Interim analysis system. This is especially likely for Lothar who was a “midget extratropical cyclone” in terms of its diameter [cf. *Ulbrich et al*., 2001].

STORM	TIME (UTC)	LAT (°E)	LON (°N)	MSLP (hPa)	dMSLP (hPa/6 std)	THRESHOLD (hPa/24 std).
Lothar	18 UTC 25 Dec. 1999	340.31	46.97	993.13	-4.56	20.26
Lothar	00 UTC 26 Dec. 1999	350.29	47.99	987.43	-5.7	20.59
Lothar	06 UTC 26 Dec. 1999	2.00	49.23	977.73	-9.7	20.99
Lothar	12 UTC 26 Dec. 1999	9.36	50.38	975.95	-1.78	21.35
Martin	00 UTC 27 Dec. 1999	335.97	46.15	1000.54	-3.71	19.99
Martin	06 UTC 27 Dec. 1999	343.94	47.08	989.73	-10.81	20.29
Martin	12 UTC 27 Dec. 1999	352.66	47.25	979.27	-10.46	20.35
Martin	18 UTC 27 Dec. 1999	359.64	47.55	968.21	-11.06	20.45
Kyrill I	06 UTC 16 Jan. 2007	293.27	43.95	1003.05	-3.02	19.23
Kyrill I	12 UTC 16 Jan. 2007	298.17	45.95	999.40	-3.65	19.92
Kyrill I	18 UTC 16 Jan. 2007	305.20	46.51	990.94	-8.46	20.11
Kyrill I	00 UTC 17 Jan. 2007	312.59	48.05	984.55	-6.39	20.61
Kyrill I	06 UTC 17 Jan. 2007	319.58	50.13	975.16	-9.39	21.27
Kyrill I	12 UTC 17 Jan. 2007	324.24	51.89	969.03	-6.13	21.81
Kyrill I	18 UTC 17 Jan. 2007	327.97	53.30	963.60	-5.43	22.22
Klaus	00 UTC 23 Jan. 2009	323.54	41.93	1003.04	-1.6	18.52
Klaus	06 UTC 23 Jan. 2009	331.20	44.07	994.07	-8.97	19.28
Klaus	12 UTC 23 Jan. 2009	338.73	45.29	982.56	-11.51	19.69
Klaus	18 UTC 23 Jan. 2009	346.81	46.35	968.61	-13.95	20.05
Klaus	00 UTC 24 Jan. 2009	353.03	46.62	965.87	-2.74	20.14
Xynthia	12 UTC 26 Feb. 2010	335.62	31.75	1000.23	-2.06	14.58
Xynthia	18 UTC 26 Feb. 2010	338.18	33.12	991.83	-8.4	15.14
Xynthia	00 UTC 27 Feb. 2010	341.59	35.40	985.73	-6.1	16.05
Xynthia	06 UTC 27 Feb. 2010	345.39	38.29	978.83	-6.9	17.17
Xynthia	12 UTC 27 Feb. 2010	349.02	41.36	974.85	-3.98	18.31
Xynthia	18 UTC 27 Feb. 2010	353.04	43.98	969.88	-4.97	19.24

Table S1. Six-hourly (TIME) latitude-longitude positions (LAT, LON) minimum mean sea-level pressures (MSLP) as derived from ERA-Interim, and corresponding MSLP tendencies (dMSLP) for the last 6 hours of the five storms discussed in the main text. The last column gives the latitude dependent 24-h THRESHOLD for explosive cyclogenesis according to *Lim and Simmonds* [2002]. Analysis times before minimum core mean-sea level pressure have been selected for which the 24h criterion of explosive cyclone deepening is fulfilled.

For the times given in Table S1, Figures S4 to S8 show maps of 300-hPa wind speed and divergence and θ_e at 850 hPa along with the storm position. The principal observations for each storm are as follows:

Lothar: Lothar crossed the polar jet stream exit region over the eastern Atlantic Ocean and benefitted from a split jet structure that caused strong upper-level divergence over the English Channel on 26 December 1999 at 06 UTC (Figure S4, left panels). At that time, Rouen in western France reported a 3-hourly pressure fall of 25.8 hPa (*Ulbrich et al.*, 2001). θ_e values at 850 hPa were between 320 and 325K to the southeast of the storm (i.e., in the warm sector), when deepening started, but barely reached 315K at the time of the most rapid deepening after 26 December 1999 at 00 UTC (Figure S4, right panels).

Martin: Martin also crossed the polar jet stream exit region over the eastern Atlantic Ocean, but the storm never came under the maximum of jet-induced upper-level divergence (Figure S5, left panels). Martin has a small area of θ_e values at 850 hPa in its vicinity that is higher than 320K at about the time when the strong deepening started at 12 UTC 25 Dec. 1999 (Figure S5, right panels).

Kyrill: Kyrill I crossed the polar jet stream exit region over the western Atlantic Ocean at the time of explosive deepening (Figure S6, left panels). The θ_e values and their aerial extent at the beginning of the explosive deepening at 16 Jan. 2007 06 UTC were comparable to those of Martin (Figure S6, right panels).

Klaus: Klaus clearly intensified while crossing the polar jet and benefitted from the upper-level divergence at the right (left) entrance of a split jet configuration (Figure S7, left panels, also *Liberato et al.* [2011]). Klaus encountered high θ_e values of about 320 K at the beginning of the explosive deepening at 23 Jan. 2009 00 UTC (Figure S7, right panels). From a Lagrangian backward trajectory analyses, *Knippertz and Wernli* [2010] noted a substantial tropical moisture export for Klaus.

Xynthia: From 26 February 2010 18 UTC onward, Xynthia approached the divergence maxima associated with the left entrance region of a polar jet streak northwest of the Iberian Peninsula at that time (Figure S8, right panels). However, the storm remained south of the jet during the next 36 hours. Xynthia is the only storm that never crossed the polar jet, though it may have benefitted from some favorable split jet configuration later in its explosive development. This can be inferred from Figure S8 on 27 February 2010 18 UTC. Yet, Xynthia explosively deepened and the high θ_e values at 850 hPa between 325 and 330 K strongly suggest the importance of "diabatic deepening" of the storm.

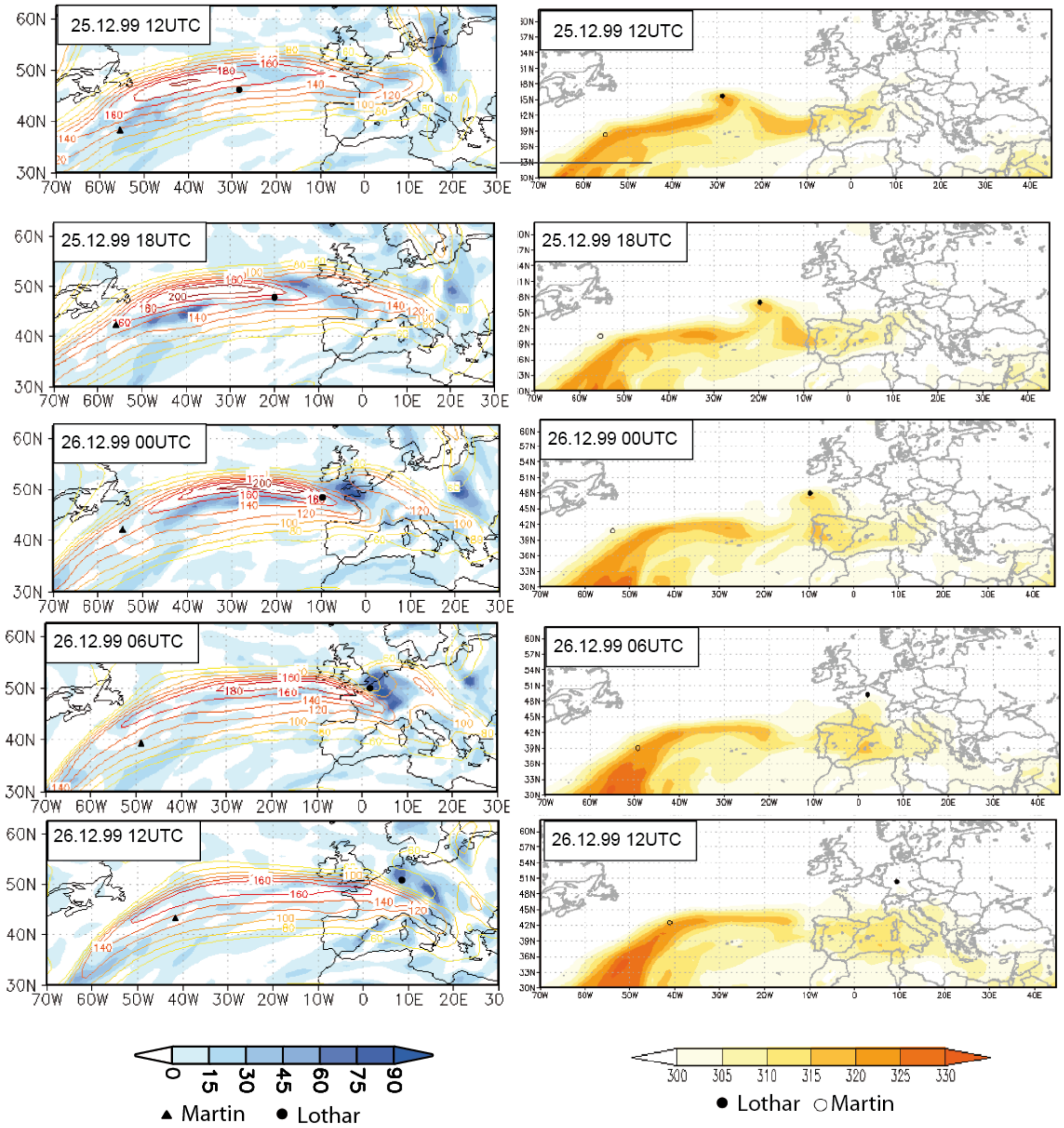

Figure S4. Storm positions relative to upper-level jets and associated divergence (left panels) and low-level air masses (right panels) for analysis times of explosive deepening of Lothar. (Left panels) Isotachs (contours every 20 Kn above the 60 Kn contour) and divergence (see color bar, in 10^{-5} s^{-1}) at 300 hPa (cf. Table S1). (Right panels) same but for θ_e at 850 hPa. θ_e was calculated after *Bolton* [1980]. The location of the storm centre is indicated by the filled circle. Martin developed just after Lothar and its position is also indicated.

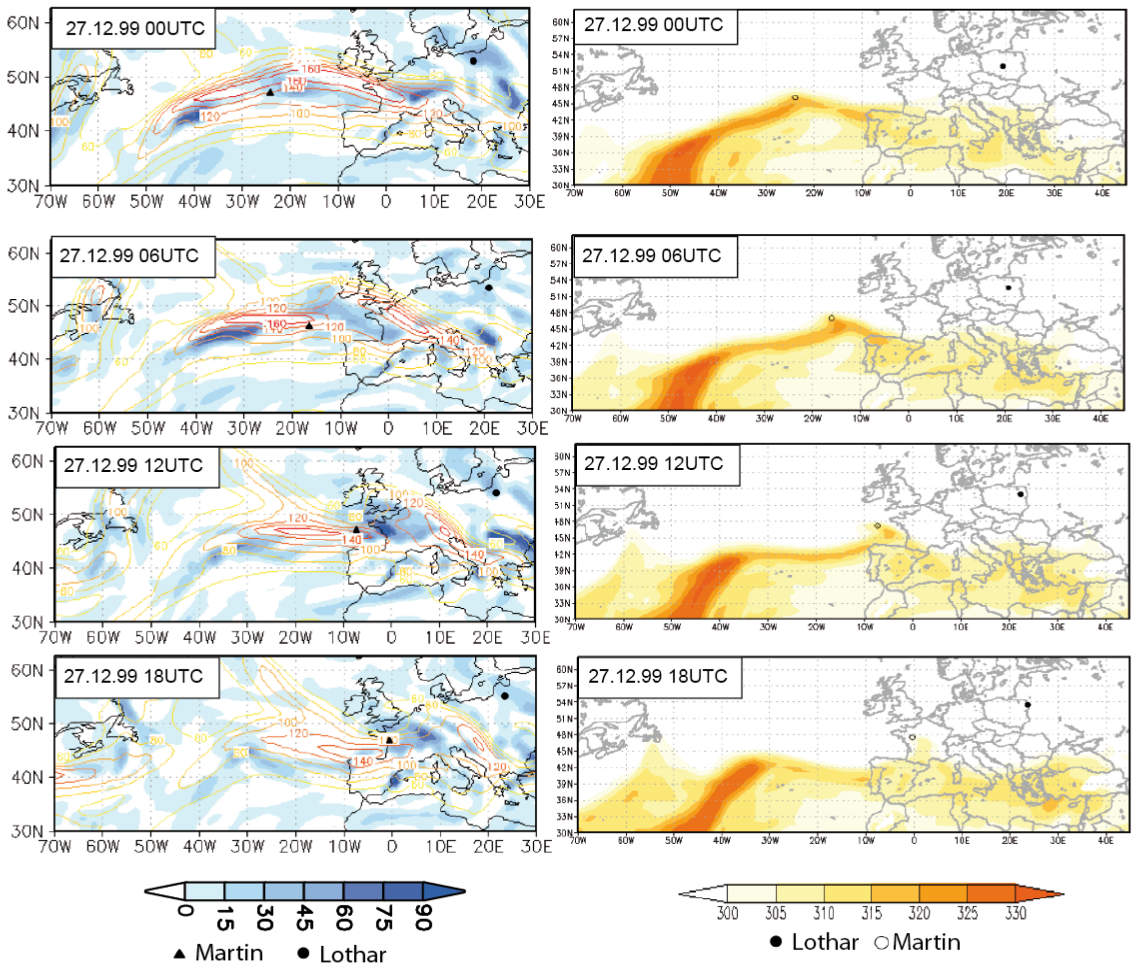

Figure S5. As in Figure S4 but for Martin

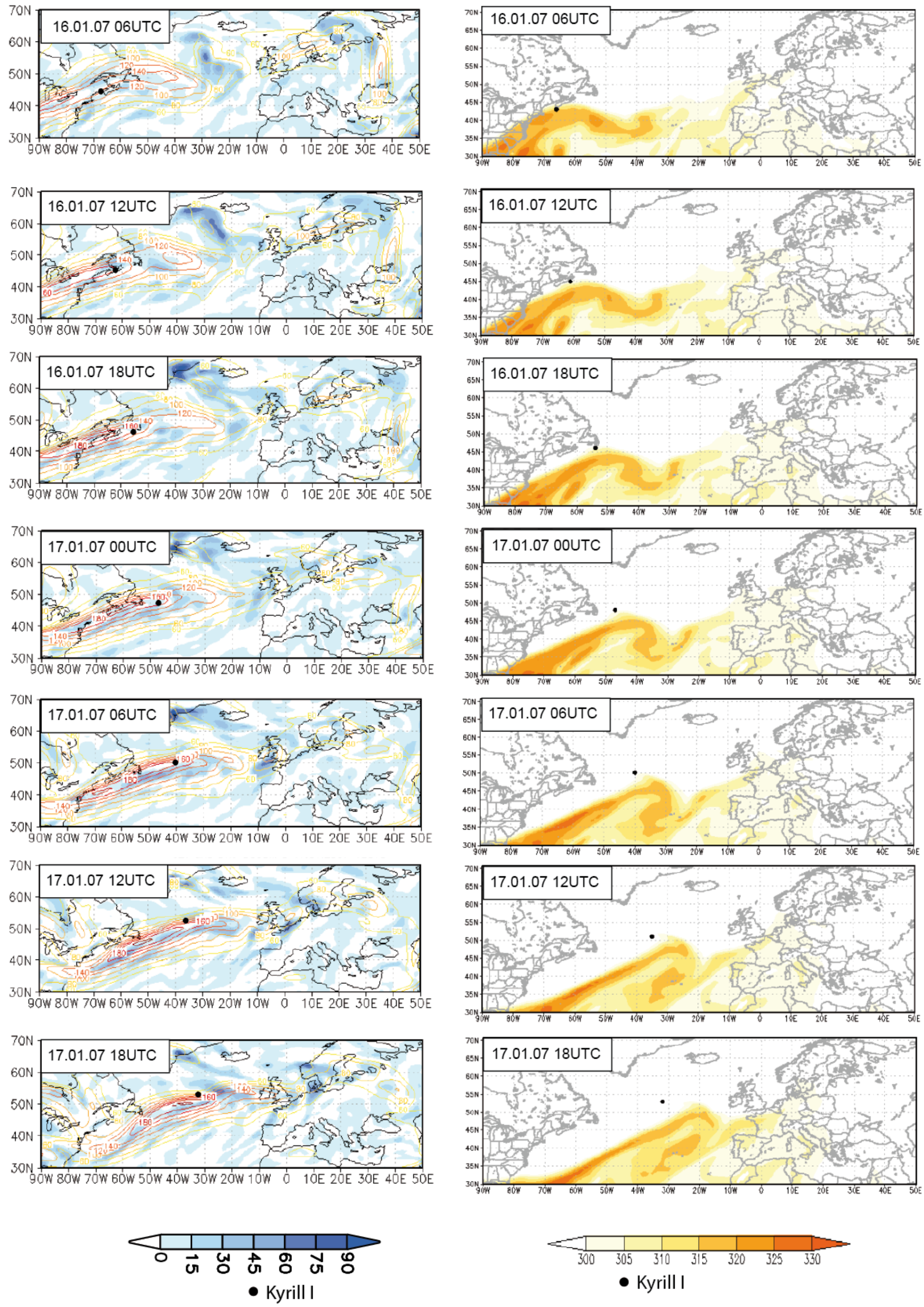

Figure S6. As in Figure S4 but for Kyrill I

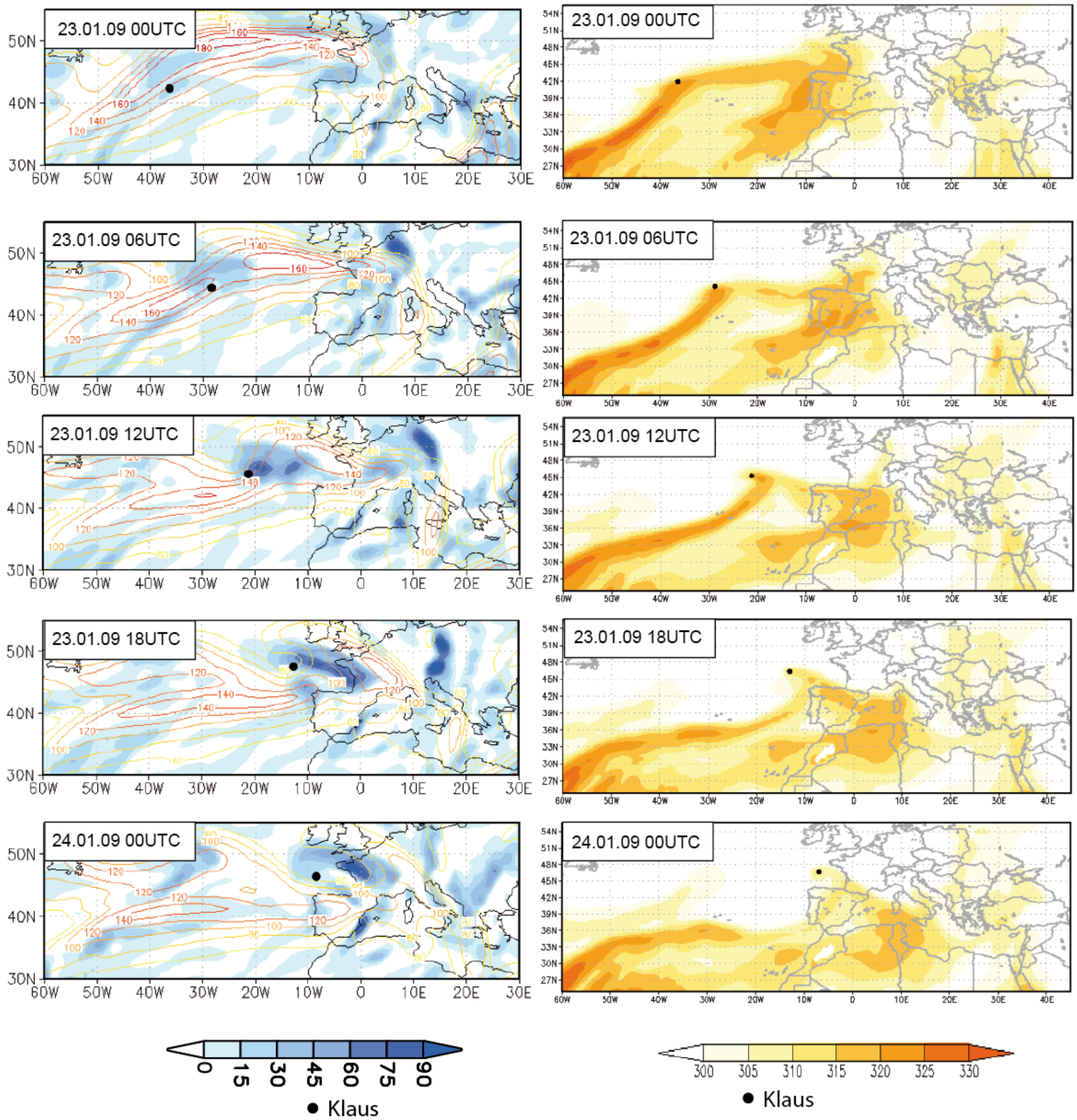

Figure S7. As in Figure S4 but for Klaus

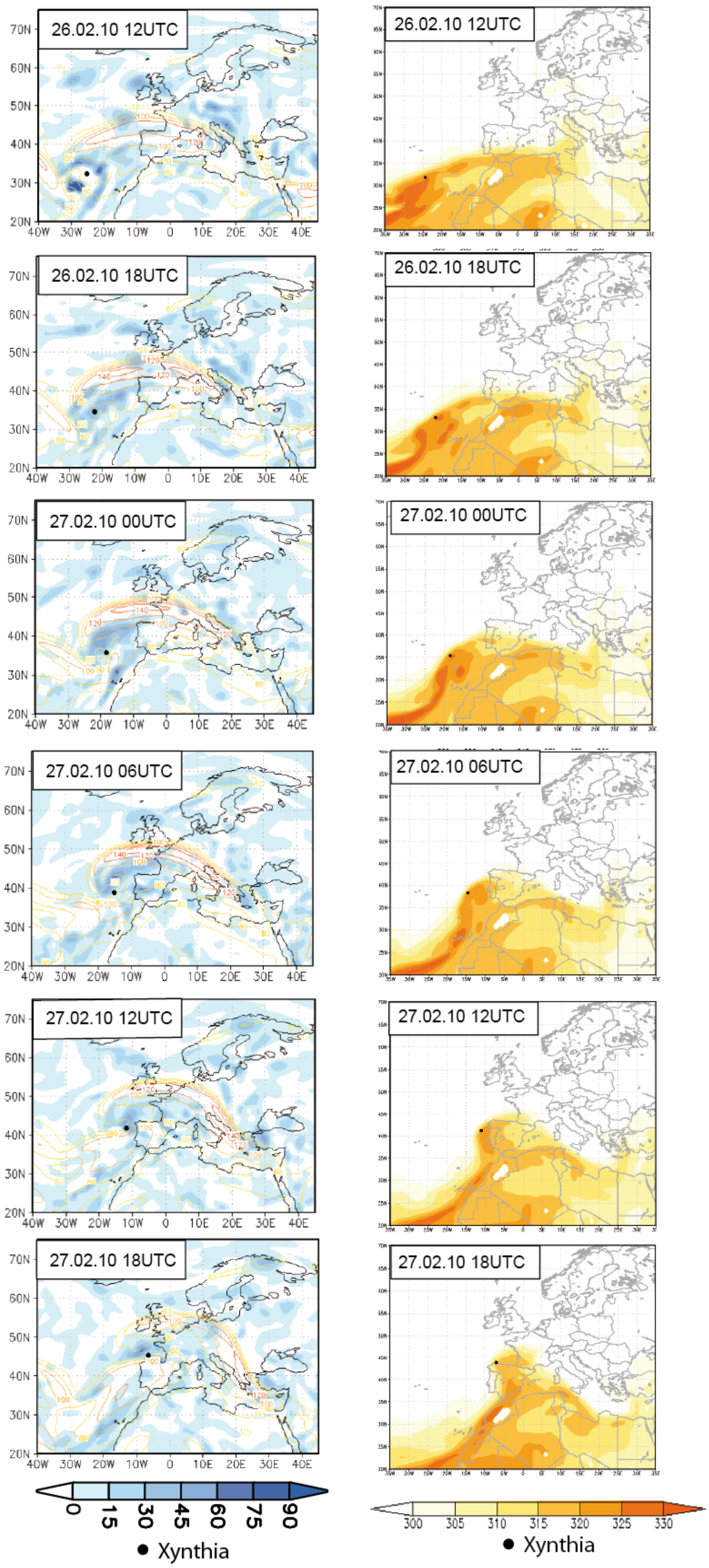

Figure S8. As in Figure S4 but for Xynthia

Acknowledgments

We acknowledge the help of Dominique Yuen in producing Figures S4–S8 and Table S1.

References

Bolton D (1980), The Computation of Equivalent Potential Temperature. *Mon. Weather Rev.,* 108, 1046–1053.

Fink, A. H., T. Brücher, E. Ermert, A. Krüger, and J. G. Pinto (2009), The European storm Kyrill in January 2007: Synoptic evolution, meteorological impacts and some considerations with respect to climate change, *Nat. Hazards Earth Syst. Sci., 9,* 405–423. doi:10.5194/nhess-9-405-2009.

Hirschberg, P. A., and J. M. Fritsch (1993), On understanding height tendencies. *Mon. Wea. Rev., 121,* 2646–2661.

Knippertz, P. und A. H. Fink (2008), Dry-Season Precipitation in Tropical West Africa and its Relation to Forcing from the Extratropics. Mon. Weather. Rev., 136, 3579–3596

Knippertz, P., A. H. Fink, and S. Pohle (2009), Reply. Mon. Weather Rev., 137, 3151–3157.

Knippertz, P., and H. Wernli (2010), A Lagrangian climatology of tropical moisture exports to the Northern Hemispheric extratropics, *J. Climate, 23,* 987–1003.

Liberato M. R. L., J. G. Pinto , I. F. Trigo , and R. M. Trigo (2011), Klaus - an exceptional winter storm over Northern Iberia and Southern France. *Weather*, *66*, 330-334, doi:10.1002/wea.755.

Lim E.-P., and I. Simmonds (2002), Explosive cyclone development in the southern hemisphere and a comparison with northern hemisphere. Mon. Weather Rev., 130, 2188–2209.

Pinto J.G., S. Zacharias, A. H. Fink, G. C. Leckebusch, and U. Ulbrich (2009), Factors contributing to the development of extreme North Atlantic cyclones and their relationship with the NAO. Clim. Dyn., 32, 711-737, doi: 10.1007/s00382-008-0396-4.

Pohle, S. (2010), Synoptische und dynamische Aspekte tropisch-extratropischer Wechselwirkungen: Drei Fallstudien von Hitzetiefentwicklungen über Westafrika während des AMMA-Experiments 2006 (In German). Ph.D. thesis at the University of Cologne, Germany, online available at http://kups.ub.uni-koeln.de/volltexte/2010/3157/pdf/DissertationSusanPohle2010.pdf.

Spengler, T., and J. Egger (2009), Comments on “Dry-Season Precipitation in Tropical West Africa and Its Relation to Forcing from the Extratropics”. Mon. Weather Rev., 137, 3149–3150.

Ulbrich, U., A. H. Fink, M. Klawa, and J. G. Pinto (2001), Three extreme storms over Europe in December 1999, Weather, 56, 70-80.